An NMR study of the role of coir fibers in the hydration and drying of cement paste at early age

Journal of Building Engineering 71 (2023) 106445

Contents lists available at ScienceDirect

Journal of Building Engineering

journal homepage: www.elsevier.com/locate/jobe

An NMR study of the role of coir fibers in the hydration and drying of cement paste at early age

XiaoXiao Zhang [a,b], MingQiang Gao [a,c], Leo Pel [a,*], David Smeulders [b]

[a] Department of Applied Physics, Eindhoven University of Technology, P. O. Box 513, 5600 MB, Eindhoven, the Netherlands
[b] Department of Mechanical Engineering, Eindhoven University of Technology, P. O. Box 513, 5600 MB, Eindhoven, the Netherlands
[c] School of Chemical Engineering and Technology, China University of Mining and Technology, Xuzhou, 221116, Jiangsu, China

ARTICLE INFO

Keywords:
Coir fibers
Hydration and drying
NMR
Water distribution
T_2/pore-size distribution

ABSTRACT

Natural fibers such as coir fibers have been increasingly explored as reinforcement in the cementitious composite to promote sustainable and economical construction. However, the in-situ application of this composite presents challenges due to the complex interplay of water behaviors, involving the hydrophilicity of natural fibers, the hydration of cement and the evaporation due to drying. Although these water-related processes play a crucial role in achieving the desired properties, they have been relatively underreported in the literature. This study aims to investigate the role of coir fibers in the water distribution and pore size distribution during the early age (initial 3 days) of cement paste hydration under drying conditions. Accordingly, Nuclear Magnetic Resonance (NMR) methods involving the moisture profiling and transverse relaxation are used to monitor the water distribution and pore size distribution in time but also in space. The samples are made by adding water-saturated coir fibers to the cement paste at different dosages (0, 1%, 2% and 4%). The effects of drying and coir fiber dosages on the samples are evaluated. The results show that drying leads to a moisture gradient and a larger transverse relaxation time T_2, i.e., a coarser pore structure near the drying surface. By adding the saturated coir fibers, the moisture gradient caused by drying is decreased and spread out along the sample. As the coir fiber content increases, the water content along the sample and the total water content of the sample increase. As a result, the samples with coir fibers exhibit a lower T_2, i.e., a denser pore structure near the drying surface. Coir fibers are shown to eliminate the adverse effect of drying on cement hydration through three effects, including the internal curing, improved water transport and crack control. The results from this study reveal the promising potential of coir fibers for in-situ construction applications.

1. Introduction

Water plays a crucial role in cement reaction. It is consumed by cement hydration to form the microstructure and hence the strength of a cement composite [1]. In in-situ practice, cement hydration is generally accompanied by a competing process, i.e., water evaporation caused by drying at the cement/air interface, resulting in the reduction of water for hydration [2]. This drying process becomes more pronounced in some cases, such as mass concrete casting and 3D printing, leading to more evaporative water loss [3]. As less water is available for the hydration of cement, coarser pores and more cracks can be introduced at the surface [4]. The resulting surface

* Corresponding author.
E-mail address: l.pel@tue.nl (L. Pel).

https://doi.org/10.1016/j.jobe.2023.106445
Received 9 January 2023; Received in revised form 15 March 2023; Accepted 30 March 2023
Available online 31 March 2023

will make the cement composite more vulnerable to the ingress of hazardous ions. For example, sulfate ions can result in the degradation of a cement matrix, and chloride ions can give rise to the corrosion of reinforcing steel bars [5]. As a result, drying during hydration will compromise the mechanical properties and durability of the cement composite [6]. In order to maintain water near the drying surface for cement hydration, one way is to apply water-entraining agents [7]. As a possible water-entraining agent, waste natural fibers, namely coir fibers, have been recently introduced owing to their cost-effective and environment-friendly advantages [8]. To facilitate the practical application of coir fibers and to achieve sustainable construction, it is of interest to explore the role of coir fibers in the hydration of cement under dry conditions.

Previous studies regarding a fresh cement composite hydrating under drying conditions have primarily focused on understanding the drying process by analyzing the resulting total water loss and evaporation rate due to drying [9–11]. The effect of factors such as water/cement ratios (w/c) and environmental conditions on the drying process has been investigated. The results show that the w/c, temperature, relative humidity and wind speed all play a role [2,10–12]. Based on the obtained evolution of total water loss and evaporation rate, the drying process in the fresh cement composite has been divided into three different stages, i.e., a constant drying rate stage, a falling drying rate stage and a low drying rate stage [11,12]. These stages are similar to those observed in the hardened cement composite and are crucial to the resulting mechanical properties of the composite [10,13–15]. In all stages, drying is found to drive water transport toward the evaporative surface of the hydrating cement composite. Since hydration occurs simultaneously, the case becomes more complicated due to the interplay between drying and hydration. The water transport caused by drying may affect the formation of the hydrate structure [9]. Meanwhile, the formed hydrate structure may influence the water transport due to drying [9]. As a consequence, both the water distribution and pore size distribution will no longer be homogenous over the cement composite but will exhibit temporal and spatial heterogeneity towards the surface. These distributions cannot be inferred by merely monitoring the total water loss due to drying. However, studies considering the water distribution and pore size distribution over time and space in the hydrating cement paste under drying conditions are relatively limited. In the presence of coir fibers, the cement reaction process under the coupled effect of hydration and drying is further complicated, as coir fibers will also interact with the water present [8]. Additionally, the water content of coir fibers affects their properties due to the influence of their chemical compositions such as lignin, hemicellulose and cellulose, and consequently, affects the interface structure between coir fibers and the cement paste [16,17]. However, to the best of the authors' knowledge, no study has reported how coir fibers affect the water behavior and pore structure in the hydrating cement paste under drying conditions.

Tracking the water distribution and pore size distribution of a hydrating fresh cement composite not only in time but also in space reduces the choice of possible measurement techniques. Nuclear Magnetic Resonance (NMR) techniques have shown advantages in delivering the relevant information with sufficient temporal and spatial resolutions in a non-destructive and non-invasive way [18]. By NMR profiling, the spatial dependence of the water distribution as well as the global water content in the hydrating cement composite can be monitored [19]. Moreover, the NMR relaxation provides additional information on the pore size distribution [20,21]. By tracking the change of different relaxation components, the water transport within the cement composite can also be obtained [22].

In this study, NMR is used to investigate the role of coir fibers in the hydration and drying of the cement paste during early age up to 3 days. Specifically, the water distribution, total water content and pore size distribution in the hydrating cement paste samples under drying conditions are measured in the absence or presence of coir fibers. The impact of drying and coir fiber contents is evaluated. To this end, simultaneous measurements are carried out on a pure hydrating cement paste sample without drying and fibers for comparison. In the following, the principle and setup of NMR are described first, then materials and experimental procedures. Subsequently, the water distribution along the sample position is obtained by measuring the moisture profile. Next, the total water content is determined from the measured moisture profile, and its loss rate is calculated to indicate the reaction kinetics in the sample. Afterward, the transverse relaxation time, the so-called T_2, which refers to the time required for the decay of the transverse magnetization, is measured at different positions in the samples. The transverse relaxation is related to the volume-to-surface ratio of water in a pore, and therefore by measuring T_2, the pore size distribution can be determined in time and space. Based on these results, the influence of drying and coir fibers on the water distribution within a hydrating cement paste and on how this water distribution affects the resulting pore size distribution are discussed. Finally, conclusions are given.

2. Methodology and materials

2.1. NMR principle

When nuclei possessing a magnetic moment, such as ^1H, are placed in a static external magnetic field B_0, their magnetic moments precess at a certain resonance frequency. This resonance frequency is called the Larmor frequency (f) which is proportional to the applied magnetic field [20]:

$$f = \gamma B_0 \tag{1}$$

where γ is the gyromagnetic ratio and is dependent on the type of nuclei ($\gamma = 42.58$ MHz/T for ^1H), and B_0 the magnitude of the static magnetic field.

If an oscillating magnetic field is introduced by a Radio Frequent (RF) pulse at the Larmor frequency of hydrogen nuclei, their magnetic moments can be manipulated. By using a Hahn RF pulse sequence, the so-called NMR spin-echo signals can be generated. The intensity of spin-echo signals is proportional to the density of hydrogen nuclei excited and therefore to the amount of water present, as given by Ref. [23]:

$$S = \rho \exp\left(-\frac{TE}{T_2}\right)\left[1 - exp\left(-\frac{TR}{T_1}\right)\right] \quad (2)$$

where ρ is the density of hydrogen nuclei, TE the spin-echo time and TR the repetition time of the spin-echo experiment, T_2 the relaxation time of transverse or spin-spin relaxation, and T_1 the relaxation time of longitudinal or spin-lattice relaxation. By combining the measured spin-echo signals at different positions in a sample, a moisture profile can be obtained.

Moreover, the decay of spin-echo signals reflects the relaxation process. The transverse relaxation can be measured with a Carr-Purcell-Meiboom-Gill (CPMG) RF pulse sequence. By analyzing with a Fast Laplace Inversion (FLI) algorithm, the spectrum of the transverse relaxation time T_2 can be recovered. It has been shown that the T_2 of pore water can be linked to the pore size [24]:

$$T_2 = \frac{1}{\rho_2}\left(\frac{V}{S}\right) \quad (3)$$

where ρ_2 is the surface relaxivity of the transverse relaxation, V the pore volume and S the pore surface area. Hence the T_2 of pore water is linearly dependent on the volume-to-surface ratio (V/S) of the pore. When pores are assumed to be spherical, V/S is equal to r/3, and T_2 is linearly dependent on the pore radius:

$$T_2 = \frac{r}{3\rho_2} \quad (4)$$

Therefore, the pore size distribution can be determined from the T_2 spectrum [20]. This method has been well established in

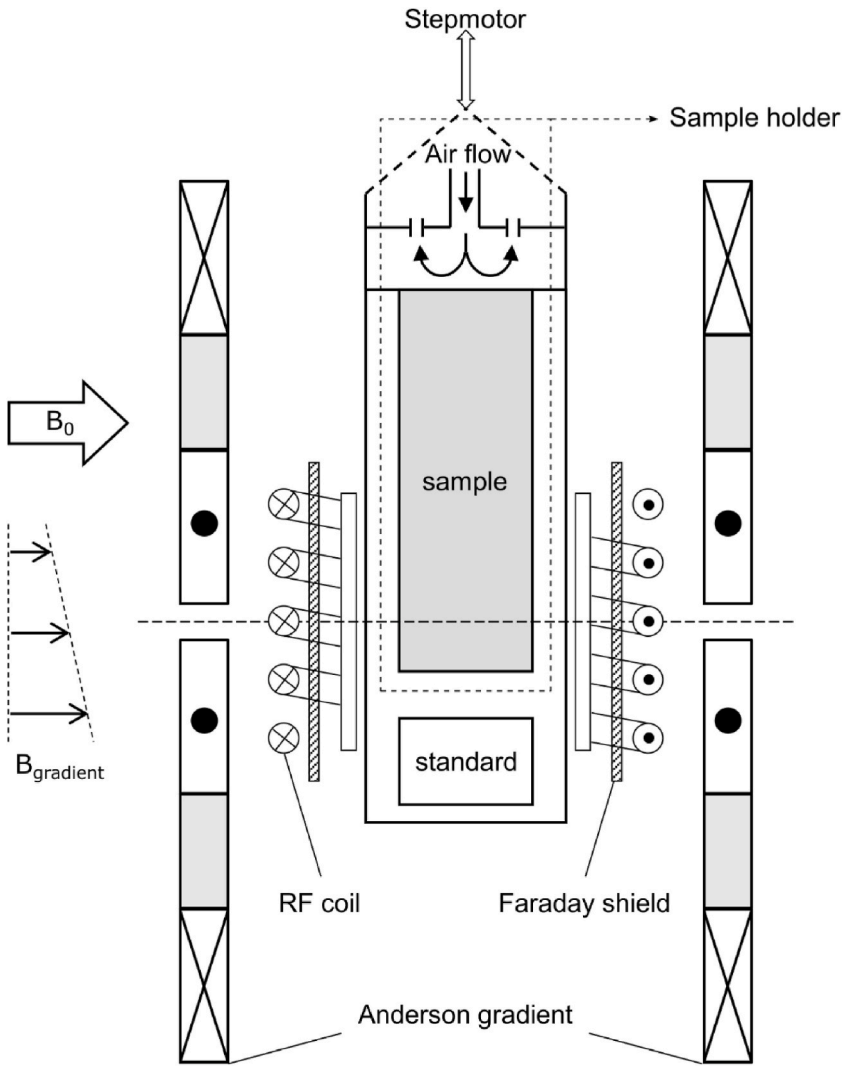

Fig. 1. A schematic representation of the NMR setup used for measuring the moisture profile and T_2 during cement hydration under drying conditions, i.e., an airflow with 0% RH. With the help of a step motor, the sample holder can be moved through the setup to be measured at different positions.

various porous materials such as cement-based materials and wood, see e.g., Refs. [20,21,25].

2.2. NMR setup

A home-built NMR setup is used in this study to measure the moisture profile and T_2 distribution. A schematic representation of the NMR setup is given in Fig. 1. The static magnetic field B_0 of 0.8 T in the horizontal direction is provided by an iron-cored electromagnet, corresponding to the resonance frequency for ^1H of 34 MHz. A constant magnetic field gradient $B_{gradient}$ of 0.3 T/m is supplied by Anderson gradient coils. The oscillating field perpendicular to the orientated field B_0 is generated by an RF coil that also receives the induced NMR signals. To accomplish a quantitative measurement of water, a Faraday shield is placed to suppress the impact of the dielectric permittivity change due to variable water contents. With a stepper motor, a sample placed in a sample holder can be moved

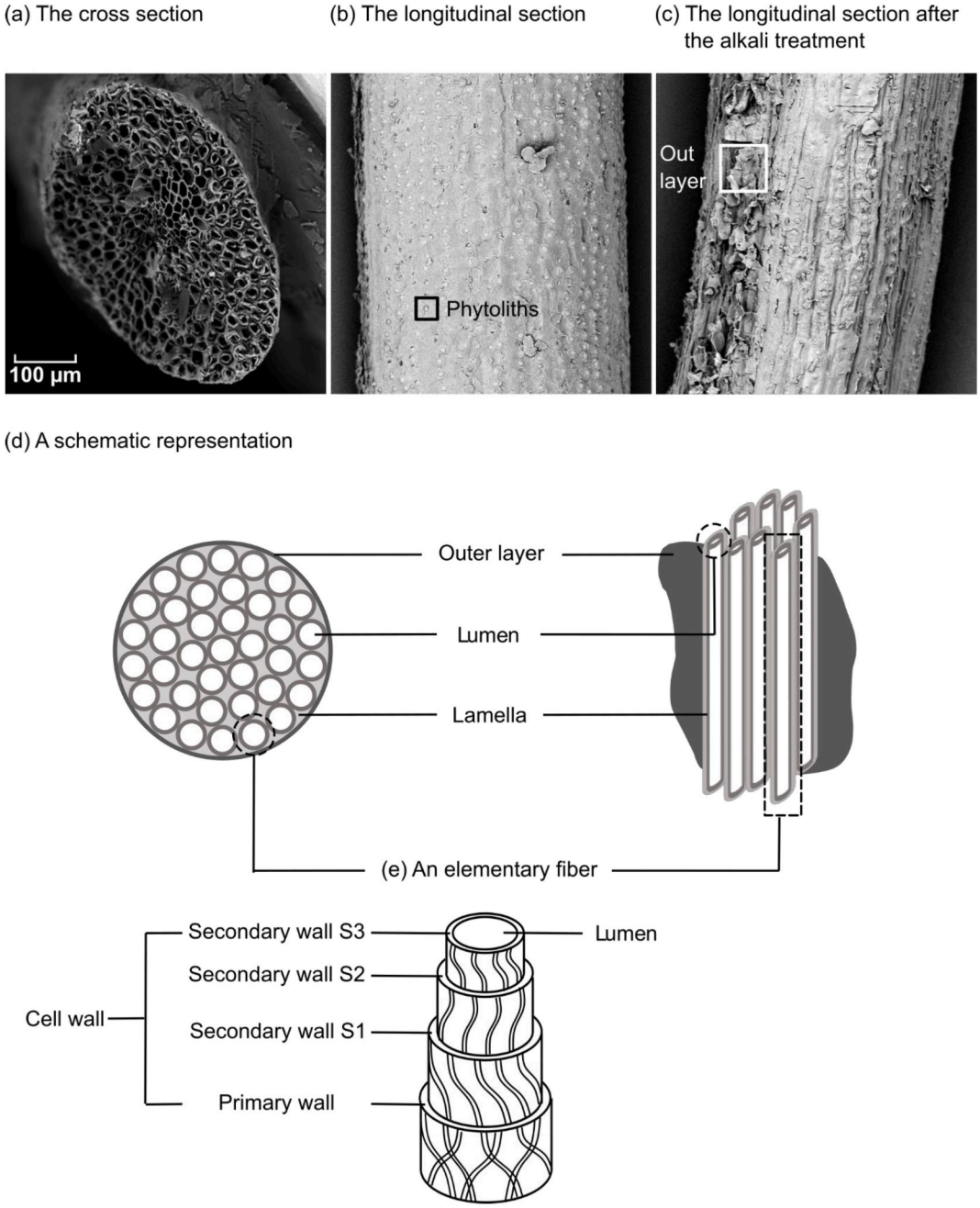

Fig. 2. The detailed microstructure of a coir fiber. (a) The cross section of a coir fiber, (b) the longitudinal section of a coir fiber and (c) the longitudinal section of an alkali-treated coir fiber, as imaged by SEM, respectively. (d) A schematic representation of a coir fiber and (e) a schematic representation of the structure of an elementary fiber of which a coir fiber is built up.

along the NMR insert to be measured at different positions. Therefore, a moisture profile can be measured along the sample height and T_2 can be measured at specific positions in the sample, i.e., the top, middle and bottom. The sample holder used is a cylindrical tube with a diameter of 25 mm and a length of 90 mm which has an open side on the top for introducing drying resulting in a 1D experiment. Drying itself is introduced by an airflow with a relative humidity (RH) of 0% and a flow rate of 1 L/min blown over the top surface of the sample. In all measurements, the spin-echo time TE is 150 μs and the repetition time TR is 5 s.

2.3. Materials and experimental procedures

In this study, the cement used is an Ordinary Portland Cement (OPC) CEM I 42.5 N. The natural fibers applied are coir fibers, provided by Wageningen Food & Biobased Research, the Netherlands. The structure of coir fibers is visualized by Scanning Electron Microscopy (SEM) at an accelerating voltage of 15 kV and is given in Fig. 2. Fig. 2a and b presents the cross section and longitudinal section, i.e., the surface morphology, of a coir fiber, respectively. The longitudinal surface of a coir fiber is covered with a layer consisting of waxes and oils and embedded with globular protrusions termed phytoliths [8,26]. To observe the internal longitudinal structure, the external layer of coir fibers is removed using an alkali treatment. In this alkali treatment, coir fibers are immersed in an 8% NaOH solution at a room temperature of 22 °C for 24 h. The alkali-treated coir fibers are obtained by filtering the solution and then drying in an oven at 40 °C for 7 days. The surface morphology of the alkali-treated coir fiber is shown in Fig. 2c. For a better understanding, a schematic representation of the structure of a coir fiber based on the obtained SEM observations is given in Fig. 2d. As can be seen, a coir fiber is made up of numerous elementary fibers [27]. Each elementary fiber is composed of various layers of cell walls and a lumen in the middle as shown in Fig. 2e [27]. All hollow elementary fibers are cemented together by lamellas and are aligned parallel in the longitudinal direction, which contributes to the porous structure of the coir fiber. The resulting structure of the coir fiber enables water to be absorbed in the fiber and transported along the fiber via its lumen. The coir fibers used in this study have an average length of 8 mm and a mean diameter in the range of 0.2–0.5 mm. More properties can be found in our previous study [19]. The coir fibers that have reached their maximum water absorption capability in the order of 130%, called saturated coir fibers, are used

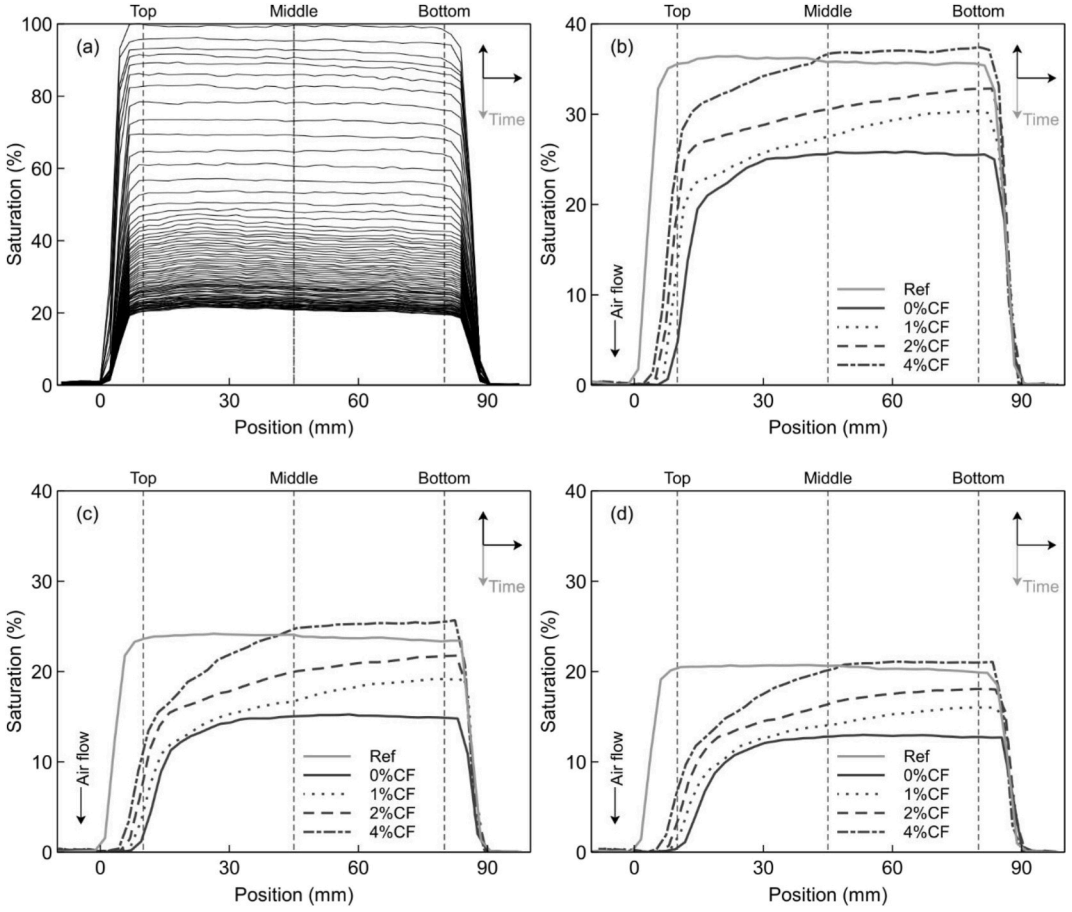

Fig. 3. The normalized moisture profile measured by NMR along the height of different samples. (a) The moisture profile measured in the reference sample. The reference sample is a pure cement paste of a w/c of 0.3 without coir fibers and drying. The moisture profile is given for a total time of 72 h (3 days). The time interval between subsequent profiles is 55 min. (b), (c) and (d) The normalized moisture profile measured in different samples at a hydration time of 24 h, 48 h and 72 h, respectively. Ref indicates the reference sample. 0%CF, 1%CF, 2%CF and 4% CF indicate the samples with 0%, 1%, 2% and 4% saturated coir fibers measured under drying conditions.

in this study to achieve the effect of internal curing.

A water/cement ratio (w/c) of 0.3 is used for all samples. Saturated coir fibers are added at 0%, 1%, 2%, and 4% by weight of cement (recorded as 0%CF, 1%CF, 2%CF and 4%CF). It should be mentioned that the water contained in saturated coir fibers is not taken into account in the w/c, as it is regarded as a part of fiber composition. In order to make a sample, first coir fibers are randomly added to cement and mixed together for 1 min. Next, water is added, and the mixing process is carried out for another 2 min. After the mixing process, the fresh cement composite is placed in the sample holder to obtain a sample with a diameter of 25 mm and a height of 90 mm. The sample holder filled with the cement sample is then immediately placed in the NMR setup for measuring under drying conditions. In addition, as a reference sample (recorded as Ref), a pure cement paste without coir fibers is measured under sealed conditions. The NMR measurement itself is started 10 min after the beginning of the mixing process. All NMR measurements are performed continuously for 72 h, i.e., 3 days, at a room temperature of 22 °C.

3. Results and discussions

3.1. Water distribution

To track the water distribution in the sample, the moisture profile is measured along the sample position using NMR. For a better comparison, the measured moisture profile is normalized with respect to the maximum moisture signal recorded. The normalized moisture profile of different samples during the reaction for up to 72 h (3 days) is shown in Fig. 3. The horizontal axis of this figure, labeled as position, corresponds to the vertical direction in Fig. 1. The three representative positions in the sample where the T_2 is measured, i.e., the top, middle and bottom, are indicated in this figure.

In Fig. 3a, the moisture profile of the reference sample, i.e., the pure cement paste without drying and fibers, is given. In total, 80 profiles have been measured continuously over the hydration time of 72 h (3 days). The time interval between subsequent profiles is in the order of 55 min. As can be seen, the moisture profile shifts downward as water is continuously consumed by cement hydration and transformed into chemical-bound water which cannot be detected by our NMR setup. It can also be seen that the moisture profile stays essentially flat along the sample position, indicating that the water is homogeneously distributed throughout the sample during the hydration.

After the introduction of drying and coir fibers, the moisture profile of different samples is plotted along with that of the reference sample at specific hydration times for comparison. The moisture profile at a hydration time of 24 h, 48 h and 72 h is given in Fig. 3b, c, and d, respectively. As can be seen, as the hydration time increases, the moisture profile goes down due to water being consumed due to both drying and hydration. However, the moisture profile no longer remains flat, suggesting that the water distribution becomes inhomogeneous.

When only drying is introduced, i.e., in the case of the 0%CF sample, the water distribution exhibits a moisture gradient near the drying surface. During both drying and hydration, water will be consumed leading to the creation of menisci and thus capillary forces in the cement paste [28]. With the continuous decrease of the water content, the capillary force acting on the cement pore structure increases [11]. As drying causes water to evaporate from the drying surface, the resulting increased capillary force on the drying surface will drive the internal water migration to the drying surface [29]. At the same time, hydration makes the cement pore structure increasingly dense which prevents water migration from the inner part to the drying surface [30]. As a result of both drying and hydration, water is not allowed to transport throughout the sample to supply the surface flux.

Once saturated coir fibers are induced, the water distribution remains inhomogeneous. Clear differences can be seen indicating the significant influence of coir fibers on the drying behavior of the cement paste. In the samples with coir fibers, the moisture gradient is

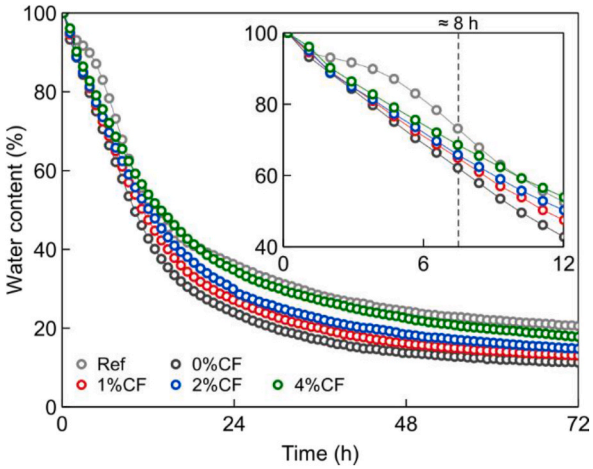

Fig. 4. The total water content in different samples as a function of the hydration time of 72 h (3 days) determined from the measured NMR moisture profile (see Fig. 3). Ref indicates the sample without coir fibers and drying. 0%CF, 1%CF, 2%CF and 4%CF indicate the samples with 0%, 1%, 2% and 4% saturated coir fibers measured under drying conditions.

spread out more evenly over the sample. With an increase in the fiber content, the saturation along the sample position increases. This observation can be attributed to the internal curing effect of saturated coir fibers as well as the enhanced internal curing effect of more coir fibers [19]. Saturated coir fibers will introduce additional water which compensates for the moisture decrease caused by hydration and drying.

3.2. Total water content and its loss rate

To get an insight into the overall water behavior, the total water content is calculated by integrating the moisture profile along the sample position and then normalizing it with respect to the initial value. The obtained total water content in various samples is plotted in Fig. 4 as a function of the hydration time.

It can be seen that in the reference sample, the total water content gradually decreases with time due to hydration. After 3 days, this decrease corresponds to a loss of 80% of the initial water content, indicating the lowest water loss among different samples.

Under drying conditions, the 0%CF sample shows the total water content decreases over time due to the combined process of hydration and drying, therefore showing a reduced water content in comparison to the reference sample. This reduction in total water content is more dominant during the initial period of the reaction. For a better observation, the total water content for the first 12 h is given in the inset of Fig. 4. As can be seen, the reduction in the total water content is much larger during the initial reaction of 8 h, i.e., the initial setting time [19]. Before the setting time, the cement paste maintains its plasticity, which allows free water to evaporate more easily. Finally, the 0%CF sample shows the largest loss of water, exhibiting an additional 8% water loss due to drying in comparison to the reference sample.

The addition of coir fibers increases the total water content of the samples during the reaction compared to the 0%CF sample. As the coir fiber content increases, the total water content also increases. Coir fibers are demonstrated to exhibit a positive effect by inhibiting the water loss in the sample caused by drying, and this effect is enhanced by a higher content of coir fibers. This phenomenon, on one hand, can be due to the internal curing effect of coir fibers, as explained in Section 3.1. On the other hand, it can be due to the crack control of coir fibers. Since coir fibers help reduce drying cracks, the water evaporation from the sample will be hindered [31].

For a better understanding of the overall water kinetics, the total water content is used to calculate the water loss rate. The water loss rate is determined by taking the derivative of the total water content with respect to time. The determined water loss rate as a function of the hydration time is given in Fig. 5.

As can be seen, the water loss rate of the reference sample reveals a four-stage reaction which is in a good agreement with the well-known hydration stages of cement [1]. During the initial 2 h, the water loss rate slows down, which is known as the induction period. After that, the water loss rate increases dramatically between 2 and 8 h, corresponding to the acceleration period. From 8 to 24 h, the water loss rate gradually reduces, which is related to the deceleration period. Later on, the water loss rate becomes almost constant, indicating the final stable period.

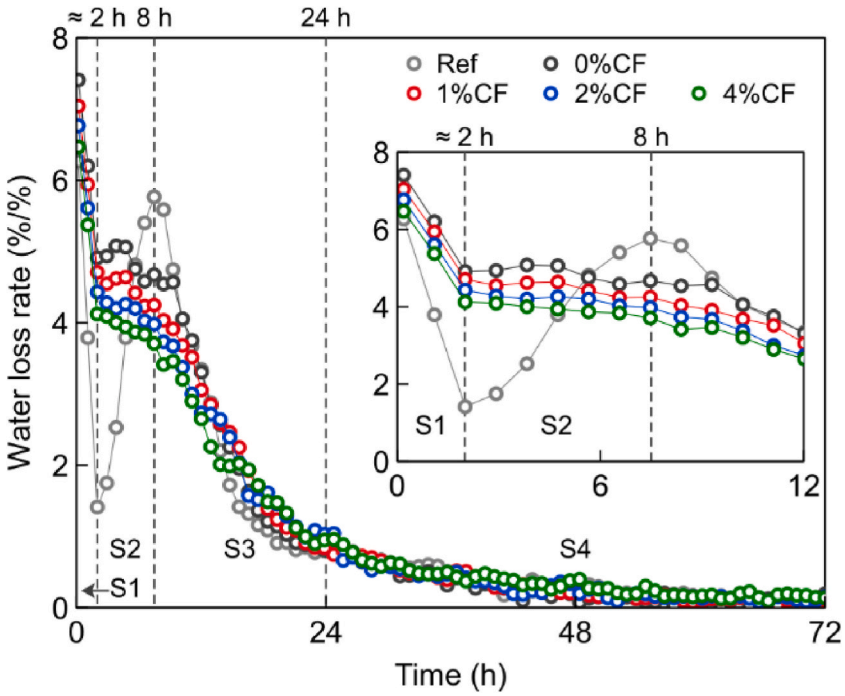

Fig. 5. The water loss rate in different samples as a function of the hydration time of 72 h (3 days) determined from the total water content (see Fig. 4). The four stages of the process are observed and indicated as S1 S2, S3 and S4, respectively. Ref indicates the sample without coir fibers and drying. 0%CF, 1%CF, 2%CF and 4%CF indicate the samples with 0%, 1%, 2% and 4% saturated coir fibers measured under drying conditions.

After the introduction of drying, the water loss rate of the 0%CF sample shows that still four stages of the reaction can be distinguished. In stage 1, i.e., the first 2 h, the water loss rate of the 0%CF sample decreases as the reference sample but remains larger. This observation suggests that drying accelerates the water loss of cement during the hydration induction period. During stage 2 between 2 and 8 h, the water loss rate of the 0%CF sample shows less variation than that of the reference sample. To better observe this variation, the water loss rate for the first 12 h is given in the inset of Fig. 5. As can be seen, the water loss rate of the 0%CF sample remains almost constant at a high rate. This observation indicates that the drying effect is significant in the hydration acceleration period of cement. From 8 to 24 h, corresponding to stage 3, the water loss rate of the 0%CF sample is reduced and becomes similar to that of the reference sample. As the cement paste changes its state from a suspension to a solid, the water transport through the sample to the drying surface becomes hindered and therefore the water evaporation shows less influence [30]. After that, in stage 4, the water loss rate of the 0%CF sample is almost stable at a low level as that of the reference sample. Drying shows a negligible influence on the loss of water.

By adding coir fibers, the water loss rate of the samples shows a similar trend as that of the 0%CF sample, again revealing four stages. With an increase in the coir fiber content, the water loss rate is slightly decreased during the first three stages. As indicated before, this phenomenon can be attributed to the internal curing effect and crack control effect of coir fibers. In addition, the coir fiber content shows a negligible influence on the water loss rate in the last stage. This change is a result of the complete depletion of the internal curing water introduced by coir fibers in the preceding stages [19].

It can be concluded that an increase in the saturated coir fibers content leads to an increase in the measured saturation and the resulting water content, therefore a decrease in the water loss rate. These changes diminish over time as water is gradually consumed by hydration and drying. Nevertheless, a higher content of coir fibers is proven not only to introduce more internal water for cement hydration but also to maintain the introduced water as well as hinder the water loss due to drying, as a result of their internal curing effect and crack control effect.

3.3. Pore size distribution

To study the effect of the water distribution on the pore size distribution, the T_2 is measured at different positions in the sample, i.e., the top, middle and bottom, as indicated in Fig. 3. Before discussing the T_2 results, the evolution of the water content at these positions is first considered, since it will directly influence the hydration reaction and the resulting pore structure, and hence the T_2 distribution. The water content at these three positions in different samples is plotted in Fig. 6 as a function of the hydration time. Moreover, for comparison, the total water content shown in Fig. 4 is also plotted in this figure.

As can be seen from Fig. 6a, in the reference sample, the water content at different positions overlaps. This observation again demonstrates the uniform water distribution, as also observed in the moisture profile given in Fig. 3. The water content at different positions also matches the total water content, indicating that no water loss due to drying is present in the reference sample.

Once drying is introduced, as shown in Fig. 6b, a clear difference can be observed in the water content of the 0%CF sample. The water content at the top position is dramatically decreased by drying and is significantly lower than that of the inner positions, i.e., the middle and bottom. The water content at the middle and bottom positions is similar, which is also similar to the total water content. This observation again shows that drying mostly affects a small zone near the exposed surface.

When coir fibers are added at the dosage of 1%, 2% and 4%, the water content obtained at different positions of the samples is shown in Fig. 6c, d and e, respectively. It can be seen that the water content at the top position increases clearly due to the presence of fibers. Moreover, the moisture gradient within the samples is reduced by adding fibers. The explanation can be that the improved water transport is introduced by coir fibers [4,8]. Owing to the porous structure of coir fibers, their addition will result in a more connected and open pore network in the hydrating cement sample. Water can be more easily transported through the sample, supplying the necessary surface flux near the drying surface and therefore reducing the moisture gradient.

To get information on the pore size distribution, the T_2 is measured at the same three positions. The T_2 distribution measured at the top position of each sample is shown in Fig. 7. In the T_2 distribution, different peaks represent the water remaining in different pore

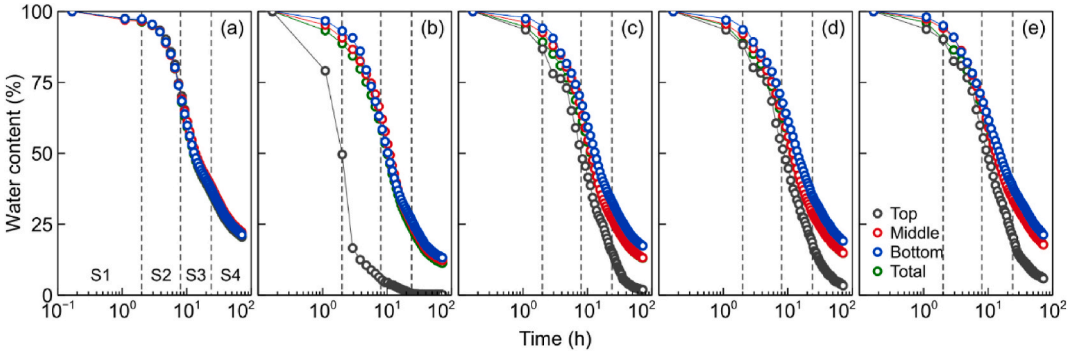

Fig. 6. The water content as a function of the hydration time of 72 h (3 days) at three different positions, i.e., the top, middle and bottom, in (a) the reference sample without coir fibers under sealed conditions, (b)–(e) the samples with 0%, 1%, 2% and 4% coir fibers under drying conditions, respectively. The total water content (see Fig. 4) is also plotted. The vertical dashed lines indicate the observed four stages, i.e., S1 S2, S3 and S4 (see Fig. 5).

sizes [20]. The amplitude of these peaks reveals the water content of the corresponding pores [19]. In addition, the measured T_2 is used to calculate the radius of pores by using Equation (4) with a surface relativity of 0.00373 nm/μs [32]. The calculated pore radius is additionally given in Fig. 7.

As seen in Fig. 7a, the T_2 distribution of the reference sample shows two peaks. The first peak, with a short T_2 value and a large area, can be associated with the water in gel pores [33]. The second peak is associated with the water located in small capillary pores whose T_2 is in the order of milliseconds [33]. These two peaks merge into one at early age and become well-resolved later on. With the

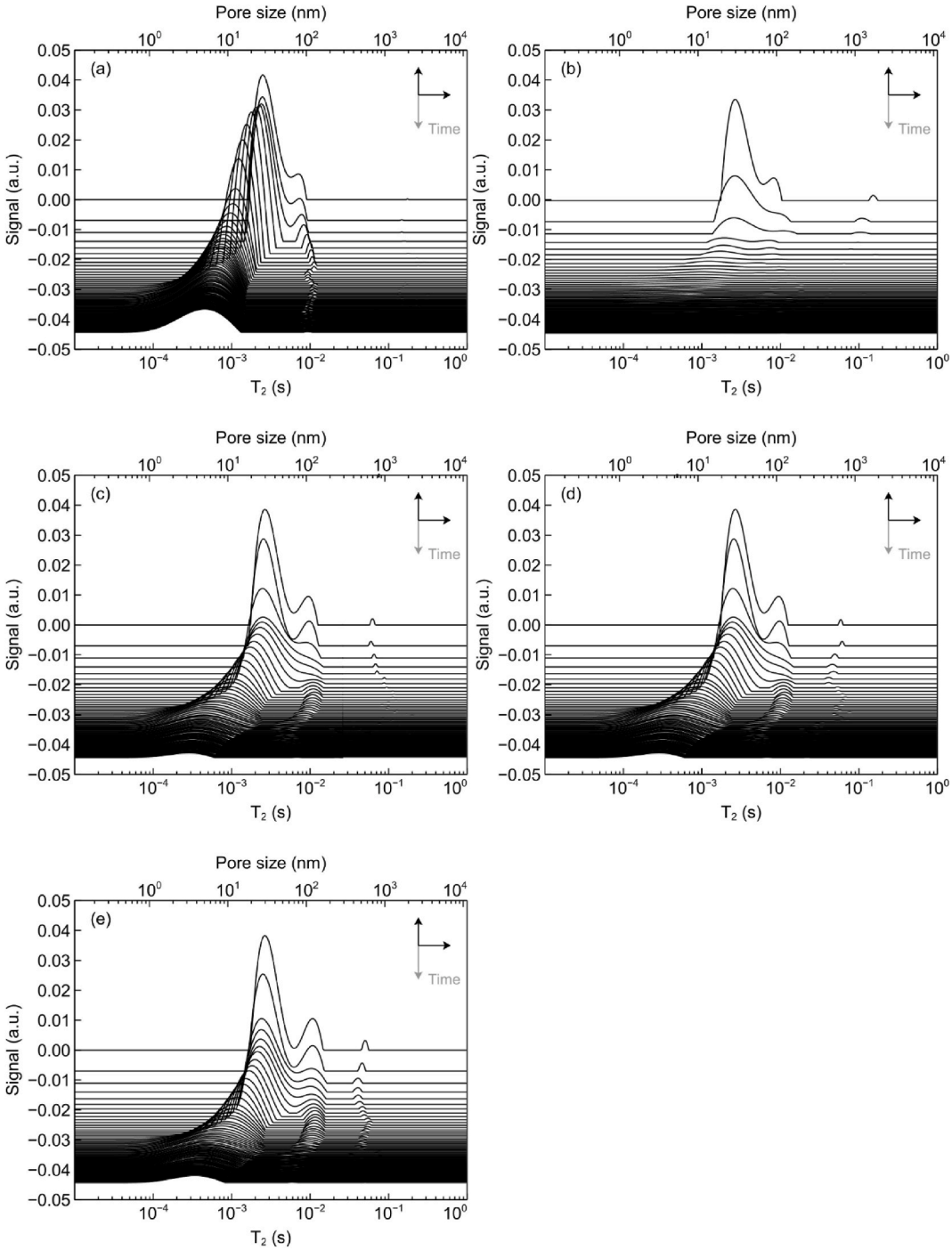

Fig. 7. The T_2/pore size distribution determined by the NMR transverse relaxation at the top position in (a) the reference sample without coir fibers under sealed conditions, (b)–(e) the samples with 0%, 1%, 2% and 4% coir fibers under drying conditions, respectively. The total time for the T_2 measurement is 72 h (3 days). The time interval between subsequent spectra is 55 min.

increased hydration time, these peaks shift towards a lower T_2 value and smaller area. This observation indicates that the size and water content of the corresponding pores are reduced during the hydration reaction. After 3 days of hydration, the second peak has disappeared and only the first peak is observed, indicating that all water present in capillary pores has been consumed by hydration.

As soon as drying is introduced, the T_2 distribution at the top position of the 0%CF sample, as given in Fig. 7b, shows significant differences. First of all, from left to right, the first two peaks, corresponding to those found in the reference sample, diminish more quickly. After several hours, these peaks are almost undetectable. This observation suggests that water is rapidly consumed as a

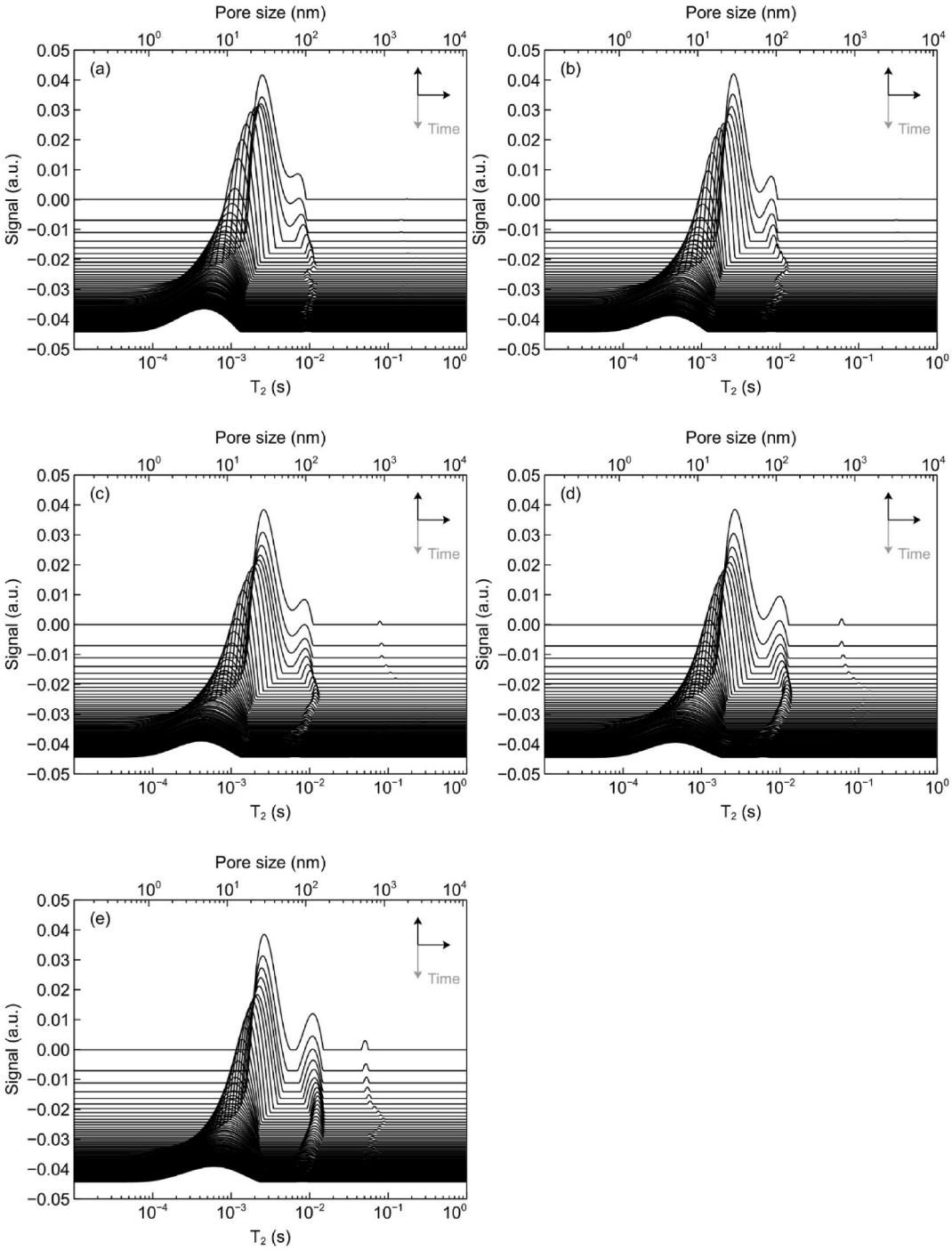

Fig. 8. The T_2/pore size distribution determined by the NMR transverse relaxation at the middle position in (a) the reference sample without coir fibers under sealed conditions, (b)–(e) the samples with 0%, 1%, 2% and 4% coir fibers under drying conditions, respectively. The total time for the T_2 measurement is 72 h (3 days). The time interval between subsequent spectra is 55 min.

consequence of drying. Due to the absence of water in pores, further changes in the T_2 cannot be observed by the NMR relaxation measurement. However, since no water is available for the further reaction with cement, it can be inferred that cement hydration will be delayed or even stopped [4]. The deterioration of cement hydration can deteriorate the pore development, leading to the formation of coarser pores. In addition, the third peak with a large T_2 value can be observed during the first 2 h, which is related to the water in large capillary pores whose T_2 value is in the order of hundreds of milliseconds [33]. The emergence of the third peak can be explained by the bleeding of the cement paste near the exposed surface caused by external drying [34].

For the samples containing 1%, 2% and 4% coir fibers, the T_2 distribution at the top position is shown in Fig. 7c, d and e, respectively. As can be seen, the T_2 distribution exhibits three peaks regardless of the fiber content. Again, the first two peaks are corresponding to those found in the 0%CF sample, referring to gel water and capillary water, respectively. However, these peaks are recorded for a larger area and a longer period in the samples with coir fibers. This change in these peaks indicates that more water is present at the top position of the sample for cement hydration, as also observed in the water content given in Fig. 6. This observation can be explained by the aforementioned effects of coir fibers including the internal curing, improved water transfer and crack control. Additionally, the third peak at a larger T_2 value is observed which can be associated with the water in medium capillary pores whose T_2 is in the order of tens of milliseconds [33]. This peak is introduced by the water contained in coir fibers. As the coir fiber content increases, this peak becomes more pronounced, i.e., the area and duration of this peak are increased. This observation indicates that more water for internal curing can be introduced by more coir fibers [8]. As hydration and drying are prolonged, all peaks gradually migrate to a lower T_2 value and a smaller area. In the end, only the first peak is observed in the samples with coir fibers. Although this peak shows a low intensity, one can still see that its T_2 covers a similar range as that of the reference sample, suggesting a similar pore size distribution.

The T_2 distribution measured at the middle position of different samples is given in Fig. 8. In the reference sample, the T_2 distribution at the middle position in Fig. 8a is almost identical to that at the top position in Fig. 7a, as a result of the uniform water distribution. The T_2 distribution of the 0%CF sample, given in Fig. 8b, exhibits a two-peak distribution that is similar to that of the reference sample. In this regard, drying shows a negligible influence on the pore structure at the middle position of the sample. For the samples with 1%, 2% and 4% coir fibers, the T_2 distribution at the middle position is shown in Fig. 8c, d and e. The T_2 distribution is similar for all the samples regardless of the fiber content, showing three peaks. Again, the sample with more coir fibers shows more pronounced T_2 peaks, indicating more internal curing water therefore an enhanced internal curing effect. As a result, an improved internal pore structure at the middle position of the sample can be expected by increasing the content of coir fibers.

At the bottom position, the T_2 distribution in the corresponding sample is similar to that at the middle position. To compare the T_2 at different positions in each sample, instead of showing the T_2 distribution at the bottom position, the T_2 value obtained from the first peak at three positions in each sample is plotted together in Fig. 9. As can be seen in Fig. 9a, the reference sample shows a uniform T_2 distribution for three different positions and therefore a similar pore size distribution, due to the uniform water distribution. As a result of drying, the inhomogeneous water distribution of the 0%CF sample is reflected in its T_2 distribution in Fig. 9b. Finally, a larger T_2 value in the order of 1.4 ms corresponding to a pore size in the order of 15 nm is obtained, suggesting coarser pores at the top position. After the introduction of coir fibers, as shown in Fig. 9c–e, the T_2 distribution is also inhomogeneous in the samples, indicating an inhomogeneous pore size distribution. As compared to the 0%CF sample, the samples with fibers have a lower T_2 value at the top position and therefore smaller pores, showing a final T_2 value in the order of 0.3 ms and a corresponding pore size in the order of 3 nm. This observation indicates that the addition of coir fibers can significantly improve the pore structure in the sample near the drying surface.

3.4. Discussion

To get a better understanding of the role of coir fibers, a schematic representation of the water behavior under the combined process of hydration and drying in the cement samples with and without coir fibers is given in Fig. 10.

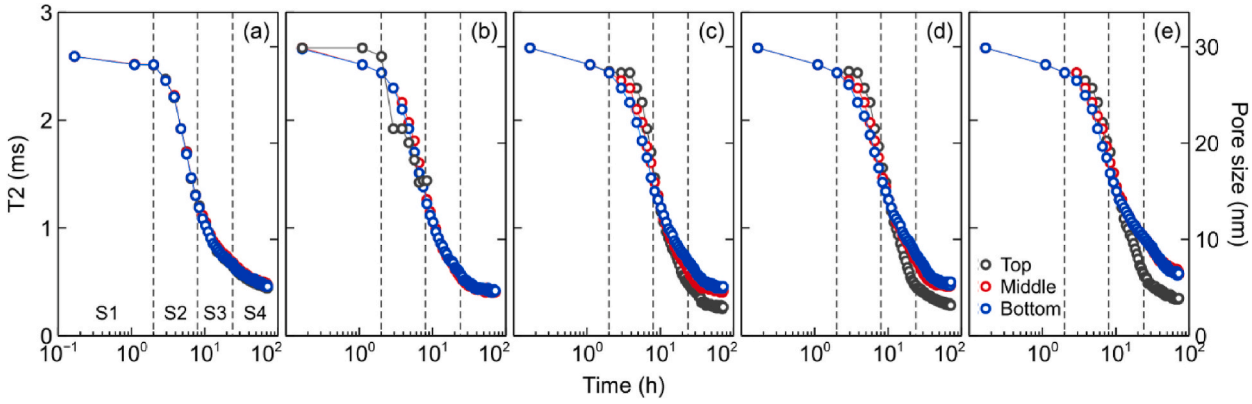

Fig. 9. The T_2 value determined from the first T_2 peak as a function of the hydration time of 72 h (3 days) at three different positions, i.e., the top, middle and bottom, in (a) the reference sample without coir fibers under sealed conditions, (b)–(e) the samples with 0%, 1%, 2% and 4% coir fibers under drying conditions, respectively. The vertical dashed lines indicate the observed four stages, i.e., S1 S2, S3 and S4 (see Fig. 5).

When only drying is introduced to a hydrating cement sample, water evaporation will occur on its surface, as shown in Fig. 10a–c. At the beginning of the combined process of hydration and drying, as shown in Fig. 10a, the sample is fully saturated and the top surface is covered by a thin water film [35]. This water film is formed due to that the settling of solid particles results in water accumulation on the sample surface, i.e., so-called bleeding. Except for the vicinity of the drying surface, the water distribution and pore size distribution in the rest part of the sample are nearly uniform. The water film becomes thinner as the reaction proceeds but no water transport is present in the sample, corresponding to the aforementioned stage 1. As water is consumed by evaporation and

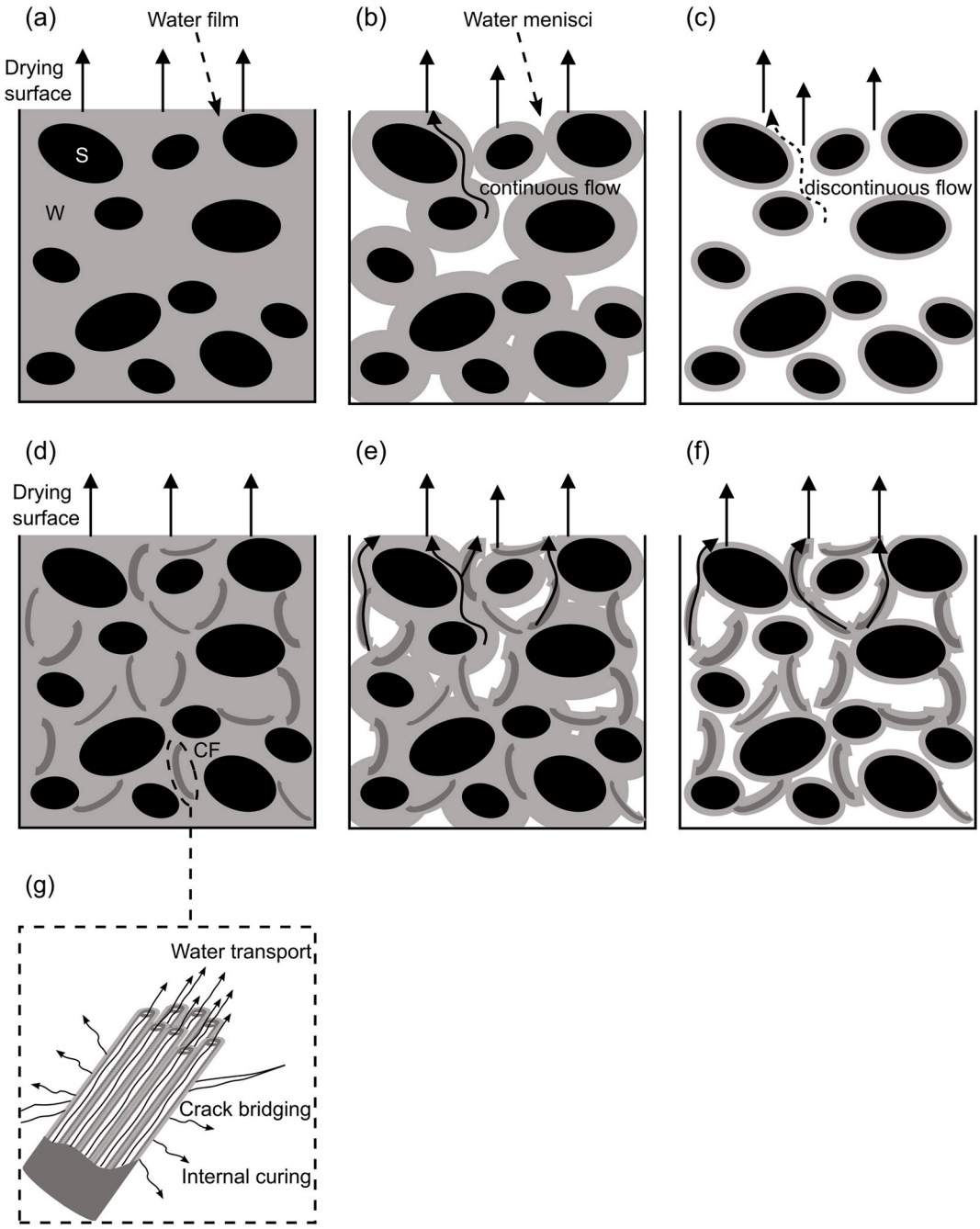

Fig. 10. A schematic representation of the water behavior of the samples in the absence or presence of coir fibers under the combined process of drying and hydration. (a)–(c) The sample without coir fibers in (a) stage 1: the sample is fully saturated with a thin water film covering on the top and no water transport is present, (b) stage 2: continuous capillary flow is generated and water can be transported to the drying surface, and (c) stage 3: discontinuous capillary flow is present and water cannot be transported to the drying surface. (d)–(f) The sample with coir fibers in (e) stage 2 and (f) stage 3 shows an increased water content and more flow paths, as a result of the three effects of saturated coir fibers, i.e., the internal curing, improved water transport and crack control. S, W and CF represent solid, water and coir fiber, respectively.

hydration, as given in Fig. 10b, the process enters stage 2. The sample becomes unsaturated and the water film on the sample surface is completely depleted. As a result, water menisci and therefore capillary pressure build up in the pores of the sample [12]. With the increase in the water loss, the curvature of the menisci increases resulting in an increase in the capillary pressure [36]. This increased capillary pressure can drive water transport from the inside toward the drying surface, making both the water distribution and pore size distribution inhomogeneous. As long as the water content and water diffusivity of the sample are sufficiently high, continuous capillary flow can be generated to support the evaporative surface flux [11]. As both drying and hydration continue, in Fig. 10c, the process reaches stage 3. As can be seen, the saturation of the sample drops continuously and the water transport is decreased by the densification of the cement pore structure. The capillary flow becomes discontinuous and is no longer able to mitigate to the drying surface [11]. Therefore, a less water content and a coarser pore structure are found in the vicinity of the drying surface. It should be mentioned that the later final stage 4 has not been shown here, as it is considered that the water flow transport is almost absent in the sample.

After the addition of saturated coir fibers, the water distribution in the cement sample is given in Fig. 10d–f. Saturated coir fibers can alter the water distribution in stage 2 and stage 3, as shown in Fig. 10e and f, in three ways. First of all, saturated coir fibers can increase the water content of the sample due to their internal curing effect, i.e., they can release the contained water to compensate for the water consumed by drying and hydration. As a result, more water is available for capillary flow and hence reaches the drying surface. Secondly, coir fibers can improve the water transport within the sample through their porous structure. The porous structure of coir fibers will provide additional transport paths for water. By using the lumens of coir fibers as channels, water can be transported to the drying surface. Additionally, coir fibers can reduce the drying cracking and therefore the water loss caused by drying of the sample. This effect has been illustrated in a previous study [19]. As less water evaporates from the sample with fewer cracks, more water is available for cement hydration. These three effects of coir fibers, i.e., the internal curing, improved water transport and crack control, are shown together in Fig. 10g. As a result of these three effects of coir fibers, more water is observed at the top position of the sample, therefore, cement can also hydrate near the drying surface, giving rise to an improved pore structure.

4. Conclusions

The use of coir fibers or other natural fibers in cementitious composites is regarded as a promising step towards achieving sustainable and economical construction. Previous studies have increasingly reported the reinforcement effect of natural fibers on the cementitious composite. Despite the reinforcement effect, the characteristics of natural fibers, i.e., the high moisture absorption capacity and porous structure, are still considered as potential obstacles to their use. However, this study provides a new insight that these characteristics can be a bonus in the case of drying through intelligent manipulation, such as saturating fibers with water.

By means of NMR 1D profiling and T_2 relaxation, the effect of saturated coir fibers on the water distribution, water content and pore size distribution of a hydrating cement paste under drying conditions has been studied during the initial 3 days. The results show that the process of cement hydration under drying conditions can be divided into 4 stages regardless of the addition of coir fibers. Drying results in an inhomogeneous water distribution showing a moisture gradient near the drying surface, and a reduced total water content for cement hydration. As a result, a larger T_2, i.e., a coarser pore structure, appears at the top position of the sample. The introduction of saturated coir fibers also leads to an inhomogeneous water distribution but a decreased moisture gradient spread out in the sample. With the increase in the fiber content, the water content along the sample as well as the total water content of the sample increases. As a consequence, a reduced T_2, i.e., a denser pore structure, is achieved at the top position of the samples with coir fibers. The incorporation of coir fibers appears to eliminate the adverse effect of drying on cement hydration. Coir fibers have been shown to improve not only the moisture distribution but the pore size distribution of the hydrating cement under drying conditions through three effects, i.e., the internal curing, improved water transport and crack control.

The results obtained in this study reveal the promising potential of coir fibers for in-situ construction applications. The results for coir fibers can be extended to other natural fibers due to their similar structure and composition. This study therefore paves the way for future studies aimed at a better understanding of the water behavior of coir fibers and other natural fibers reinforced cementitious composites. It also demonstrates the capabilities of non-destructive and non-invasive NMR in monitoring water distribution and pore size distribution dynamically in time and space. The use of NMR further advances the identification of coir fibers and other natural fibers in cementitious composites beyond the current state of knowledge. However, this study focuses on the early performance of the coir fibers and cement composites, further studies are necessary to understand their long-term performance. Along with this issue, the main drawback of this material is raised by the lack of durability of natural fibers in the alkaline cementitious environment. To mitigate this drawback, approaches such as fiber pre-treatment and matrix modification need to be investigated. In addition, other types of natural fibers are needed to be explored for their potential in the internal curing technology.

Author statement

All persons who meet authorship criteria are listed as authors, and all authors certify that they take public responsibility for the content. The specific contributions made by each author are indicated as below:

XiaoXiao Zhang: Conceptualization; Methodology; Performing experiments; Validation; Writing- Original draft preparation; Writing - Review & Editing.**MingQiang Gao**: Writing - Review & Editing.**Leo Pel**: Conceptualization; Supervision; Writing - Review & Editing.**David Smeulders**: Supervision; Writing - Review & Editing.

Declaration of competing interest

The authors declare that they have no known competing financial interests or personal relationships that could have appeared to influence the work reported in this paper.

Data availability

Data will be made available on request.

Acknowledgements

This research is supported by the China Scholarship Council (Grant No. 201708410130) and the Eindhoven University of Technology. Part of this work is carried out in the Darcy Center for porous media research at the Eindhoven University of Technology.

References

[1] H.F.W. Taylor, Cement Chemistry, second ed., 1997, https://doi.org/10.1680/cc.25929.
[2] W.J. McCarter, A.M. Ben-Saleh, Influence of practical curing methods on evaporation of water from freshly placed concrete in hot climates, Build. Environ. 36 (2001) 919–924, https://doi.org/10.1016/S0360-1323(00)00048-2.
[3] M.T. Souza, I.M. Ferreira, E. Guzi de Moraes, L. Senff, A.P. Novaes de Oliveira, 3D printed concrete for large-scale buildings: an overview of rheology, printing parameters, chemical admixtures, reinforcements, and economic and environmental prospects, J. Build. Eng. 32 (2020), https://doi.org/10.1016/j.jobe.2020.101833.
[4] J. Liu, N. Farzadnia, C. Shi, X. Ma, Effects of superabsorbent polymer on shrinkage properties of ultra-high strength concrete under drying condition, Construct. Build. Mater. 215 (2019) 799–811, https://doi.org/10.1016/j.conbuildmat.2019.04.237.
[5] Y. Wei, X. Zheng, W. Guo, Shrinkage, strength development and cracking of internally cured concrete exposed to dry conditions, J. Build. Mater. 19 (2016) 902–908, https://doi.org/10.3969/j.issn.1007-9629.2016.05.020.
[6] X.Y. Wang, K.B. Park, Analysis of the compressive strength development of concrete considering the interactions between hydration and drying, Cement Concr. Res. 102 (2017) 1–15, https://doi.org/10.1016/j.cemconres.2017.08.010.
[7] N.P. Tran, C. Gunasekara, D.W. Law, S. Houshyar, S. Setunge, A. Cwirzen, A critical review on drying shrinkage mitigation strategies in cement-based materials, J. Build. Eng. 38 (2021), 102210, https://doi.org/10.1016/j.jobe.2021.102210.
[8] X. Zhang, L. Pel, F. Gauvin, D. Smeulders, Reinforcing mechanisms of coir fibers in light-weight aggregate concrete, Materials 14 (2021) 1–20, https://doi.org/10.3390/ma14030699.
[9] M. Bakhshi, B. Mobasher, Experimental observations of early-age drying of Portland cement paste under low-pressure conditions, Cem. Concr. Compos. 33 (2011) 474–484, https://doi.org/10.1016/j.cemconcomp.2011.01.009.
[10] M. Azenha, K. Maekawa, T. Ishida, R. Faria, Drying induced moisture losses from mortar to the environment. Part I: experimental research, Mater, Struct. Constr. 40 (2007) 801–811, https://doi.org/10.1617/s11527-007-9244-y.
[11] M. Bakhshi, B. Mobasher, C. Soranakom, Moisture loss characteristics of cement-based materials under early-age drying and shrinkage conditions, Construct. Build. Mater. 30 (2012) 413–425, https://doi.org/10.1016/j.conbuildmat.2011.11.015.
[12] Y. Wei, W. Guo, Q. Zhang, A model for predicting evaporation from fresh concrete surface during the plastic stage, Dry. Technol. 38 (2020) 2231–2241, https://doi.org/10.1080/07373937.2019.1691012.
[13] D. Cao, S. Malakooti, V.N. Kulkarni, Y. Ren, H. Lu, Nanoindentation measurement of core–skin interphase viscoelastic properties in a sandwich glass composite, Mech. Time-Dependent Mater. 25 (2021) 353–363, https://doi.org/10.1007/s11043-020-09448-y.
[14] D. Cao, S. Malakooti, V.N. Kulkarni, Y. Ren, Y. Liu, X. Nie, D. Qian, D.T. Griffith, H. Lu, The effect of resin uptake on the flexural properties of compression molded sandwich composites, Wind Energy 25 (2022) 71–93, https://doi.org/10.1002/we.2661.
[15] X. Wang, T. Xu, M.J. de Andrade, I. Rampalli, D. Cao, M. Haque, S. Roy, R.H. Baughman, H. Lu, The interfacial shear strength of carbon nanotube sheet modified carbon fiber composites, in: Conf. Proc. Soc. Exp. Mech. Ser., 2021, pp. 25–32, https://doi.org/10.1007/978-3-030-59542-5_4.
[16] N.G. Jústiz-Smith, G.J. Virgo, V.E. Buchanan, Potential of Jamaican banana, coconut coir and bagasse fibres as composite materials, Mater. Char. 59 (2008) 1273–1278, https://doi.org/10.1016/j.matchar.2007.10.011.
[17] M. Ali, X. Li, N. Chouw, Experimental investigations on bond strength between coconut fibre and concrete, Mater. Des. 44 (2013) 596–605, https://doi.org/10.1016/j.matdes.2012.08.038.
[18] S.D. Beyea, B.J. Balcom, T.W. Bremner, R.L. Armstrong, P.E. Grattan-Bellew, Detection of drying-induced microcracking in cementitious materials with space-resolved 1H nuclear magnetic resonance relaxometry, J. Am. Ceram. Soc. 86 (2003) 800–805, https://doi.org/10.1111/j.1151-2916.2003.tb03378.x.
[19] X.X. Zhang, Y.L. Ji, L. Pel, Z.P. Sun, D. Smeulders, Early-age hydration and shrinkage of cement paste with coir fibers as studied by Nuclear Magnetic Resonance, Construct. Build. Mater. 336 (2022), 127460, https://doi.org/10.1016/j.conbuildmat.2022.127460.
[20] R.M.E. Valckenborg, L. Pel, K. Hazrati, K. Kopinga, J. Marchand, Pore water distribution in mortar during drying as determined by NMR, Mater, Struct. Constr 34 (2001) 599–604, https://doi.org/10.1007/bf02482126.
[21] P.F. de, A.E. Marble, B.J. Balcom, J.C. García, I.V. Masthikin, M.D.A. Thomas, T.W. Bremner, Embedded NMR sensors to monitor evaporable water loss caused by hydration and drying in Portland cement mortar, Cement Concr. Res. 39 (2009) 324–328, https://doi.org/10.1016/j.cemconres.2009.01.011.
[22] D. Snoeck, L. Pel, N. De Belie, Superabsorbent polymers to mitigate plastic drying shrinkage in a cement paste as studied by NMR, Cem. Concr. Compos. 93 (2018) 54–62, https://doi.org/10.1016/j.cemconcomp.2018.06.019.
[23] E.L. Hahn, Spin echoes, Phys. Rev. E 80 (1950) 580–594, https://doi.org/10.1103/PhysRev.80.580.
[24] K.R. Brownstein, C.E. Tarr, Importance of classical diffusion in NMR studies of water in biological cells, Phys. Rev. 19 (1979) 2446–2453, https://doi.org/10.1103/PhysRevA.19.2446.
[25] G. Almeida, S. Gagné, R.E. Hernández, A NMR study of water distribution in hardwoods at several equilibrium moisture contents, Wood Sci. Technol. 41 (2007) 293–307, https://doi.org/10.1007/s00226-006-0116-3.
[26] K.C.C. Carvalho, D.R. Mulinari, H.J.C. Voorwald, M.O.H. Cioffi, Chemical modification effect on the mechanical properties of hips/coconut fiber composites, Bioresources 5 (2010) 1143–1155.
[27] L. Yan, N. Chouw, L. Huang, B. Kasal, Effect of alkali treatment on microstructure and mechanical properties of coir fibres, coir fibre reinforced-polymer composites and reinforced-cementitious composites, Construct. Build. Mater. 112 (2016) 168–182, https://doi.org/10.1016/j.conbuildmat.2016.02.182.
[28] S. Tang, D. Huang, Z. He, A review of autogenous shrinkage models of concrete, J. Build. Eng. 44 (2021), 103412, https://doi.org/10.1016/j.jobe.2021.103412.
[29] Z. Jiang, Y. Xi, X. Gu, Q. Huang, W. Zhang, Modelling of water vapour sorption hysteresis of cement-based materials based on pore size distribution, Cement Concr. Res. 115 (2019) 8–19, https://doi.org/10.1016/j.cemconres.2018.09.015.
[30] A. Zhang, W. Yang, Y. Ge, Y. Wang, P. Liu, Study on the hydration and moisture transport of white cement containing nanomaterials by using low field nuclear magnetic resonance, Construct. Build. Mater. 249 (2020), 118788, https://doi.org/10.1016/j.conbuildmat.2020.118788.
[31] C.L. Hwang, V.A. Tran, J.W. Hong, Y.C. Hsieh, Effects of short coconut fiber on the mechanical properties, plastic cracking behavior, and impact resistance of cementitious composites, Construct. Build. Mater. 127 (2016) 984–992, https://doi.org/10.1016/j.conbuildmat.2016.09.118.

[32] D. Snoeck, L. Pel, N. De Belie, Comparison of different techniques to study the nanostructure and the microstructure of cementitious materials with and without superabsorbent polymers, Constr. Build. Mater. 223 (2019) 244–253. https://doi.org/10.1016/j.conbuildmat.2019.06.225.
[33] E. Jumate, D. Moldovan, D.L. Manea, D.E. Demco, R. Fechete, The effects of cellulose ethers and limestone fillers in Portland cement-based mortars by 1H NMR relaxometry, Appl. Magn. Reson. 47 (2016) 1353–1373, https://doi.org/10.1007/s00723-016-0844-y.
[34] Y. Ji, L. Pel, Z. Sun, The microstructure development during bleeding of cement paste: an NMR study, Cement Concr. Res. 125 (2019), 105866, https://doi.org/10.1016/j.cemconres.2019.105866.
[35] A. Jamali, J. Mendes, B. Nagaratnam, M. Lim, A new four stage model of capillary pressure in early age concrete: insights from high capacity tensiometers, Cement Concr. Res. 161 (2022), 106955, https://doi.org/10.1016/j.cemconres.2022.106955.
[36] V. Slowik, M. Schmidt, R. Fritzsch, Capillary pressure in fresh cement-based materials and identification of the air entry value, Cem. Concr. Compos. 30 (2008) 557–565, https://doi.org/10.1016/j.cemconcomp.2008.03.002.